Modeling error evaluation for the viscoelastic full waveform inversion

Tianze Zhang*, Kristopher Innanen, and Daniel Trad
zhang.tianze@ucalgary.ca

INTRODUCTION

In the traditional viscoelastic Full Waveform Inversion (FWI) approach based on the generalized standard linear solid (GSLS) model, the quality factor, denoted as Q, is not directly inverted. Instead, it is first converted into a set of relaxation variables. Thus, the viscoelastic FWI process involves inverting for both elastic and relaxation models and translating the relaxation variables back into the Q model to achieve the final inversion results. In this report, we propose a novel method where a Multi-Layer Perceptron (MLP) is pre-trained to learn the mapping from Q values to relaxation variables. This trained MLP is then integrated into a Recurrent Neural Network (RNN)-based GSLS viscoelastic FWI framework, creating a complete computational graph, thereby enabling the direct inversion of the Q model. Additionally, we employ the Monte Carlo dropout technique within the neural network to quantify the uncertainty associated with the MLP's learning process for mapping Q values to relaxation variables. Our observations suggest that this modeling error primarily affects the attenuation models. The findings of this study have significant implications for improving the accuracy and reliability of viscoelastic FWI, particularly in how we understand and handle the inherent uncertainties in modeling complex subsurface properties.

METHODOLOGY

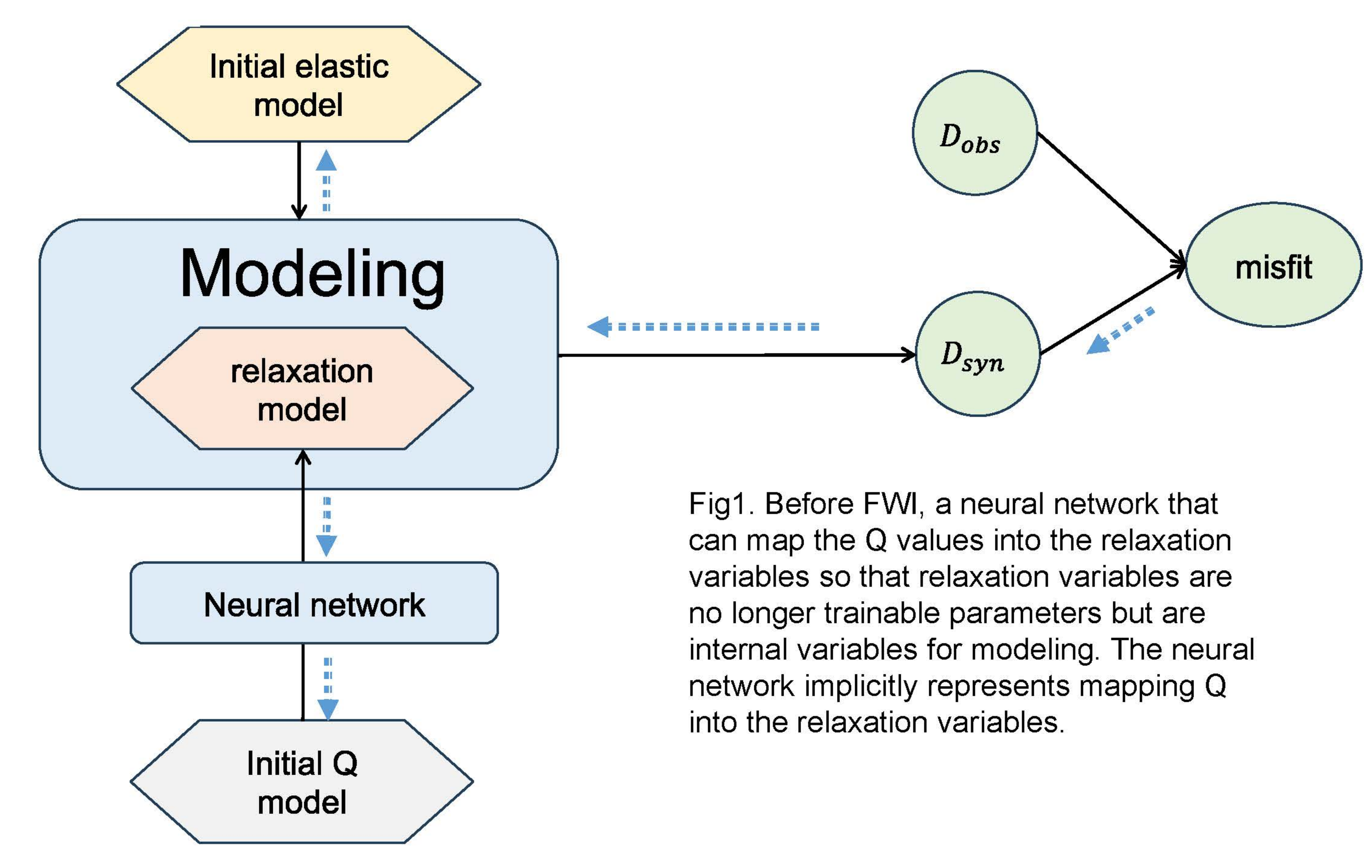

Fig1. Before FWI, a neural network that can map the Q values into the relaxation variables so that relaxation variables are no longer trainable parameters but are internal variables for modeling. The neural network implicitly represents mapping Q into the relaxation variables.

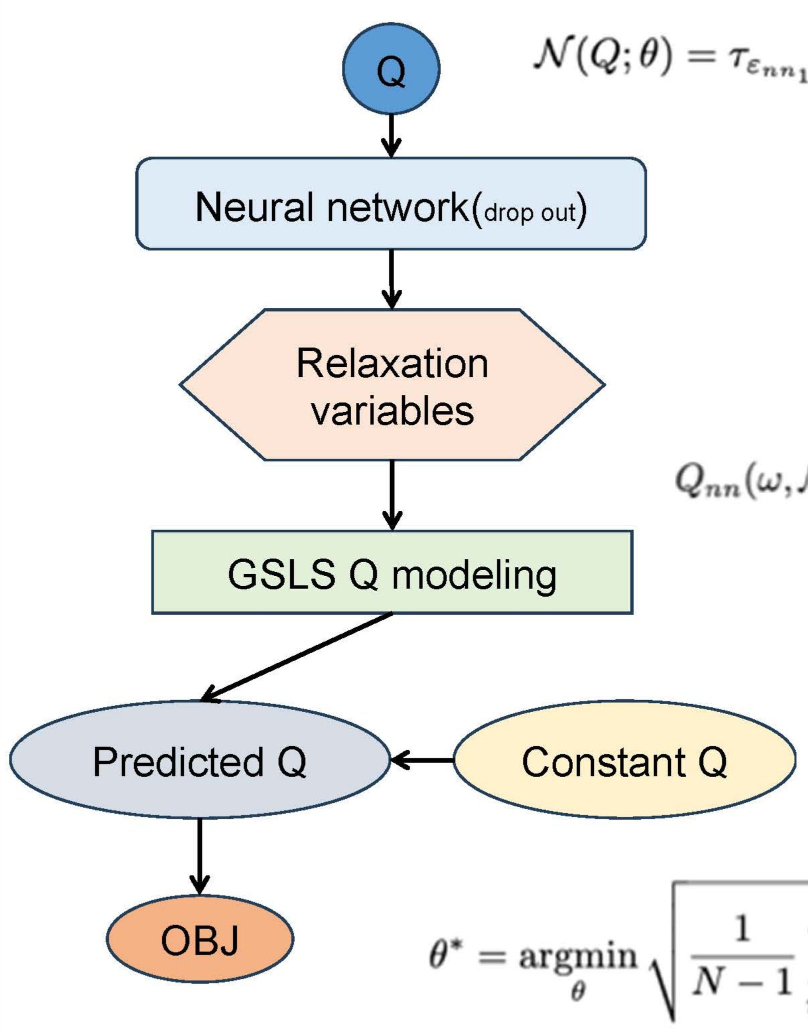

$$\mathcal{N}(Q;\theta) = \tau_{\varepsilon_{nn_1}}, \tau_{\sigma_{nn_1}}, \tau_{\varepsilon_{nn_2}}, \tau_{\sigma_{nn_2}}, \cdots, \tau_{\varepsilon_{nn_L}}, \tau_{\sigma_{nn_L}},$$

$$Q_{nn}(\omega, \mathcal{N}(Q;\theta)) = \frac{1 - L + \sum_{l=1}^{L} \frac{1+\omega^2 \tau_{\varepsilon_{nn_l}} \tau_{\sigma_{nn_l}}}{1+\omega^2 \tau_{\sigma_{nn_l}}^2}}{\sum_{l=1}^{L} \frac{\omega\left(\tau_{\varepsilon_{nn_l}} - \tau_{\sigma_{nn_l}}\right)}{1+\omega^2 \tau_{\sigma_{nn_l}}^2}}$$

$$\theta^* = \underset{\theta}{\operatorname{argmin}} \sqrt{\frac{1}{N-1} \sum_{n=1}^{N} \left[\frac{1}{Q_{nn}\left(\omega_n, \mathcal{N}(Q;\theta)\right)} - \frac{1}{Q_{\text{true}}(\omega_n)}\right]^2}.$$

Fig2. Illustration for how to train the neural network to generate the relaxation variables for the constant Q model under GSLS mechanism.

NUMERICAL TESTS

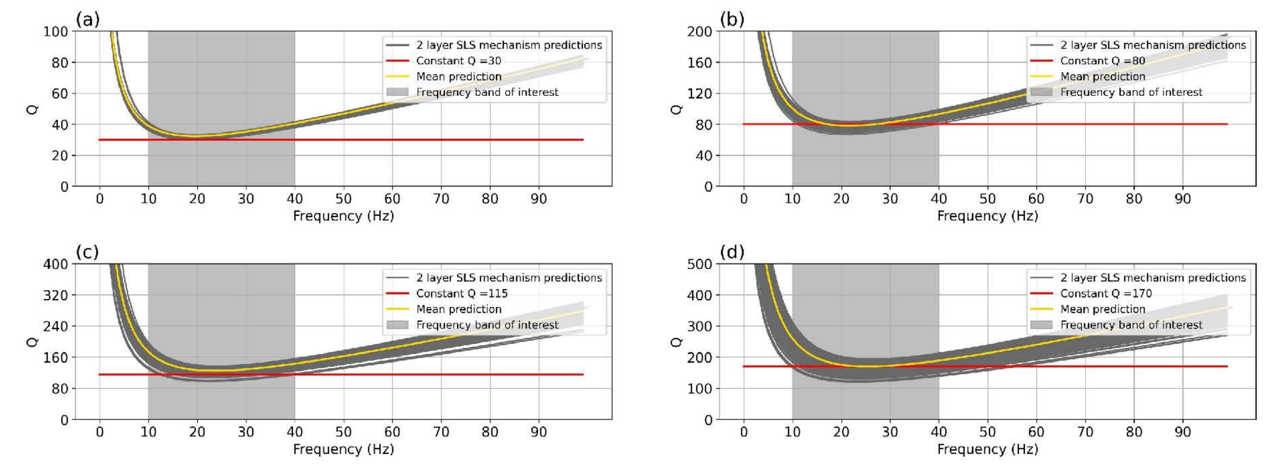

Fig3. The Q spectrums and the uncertainty quantification predicted by the neural network using 2 layers of the GSLS mechanism.

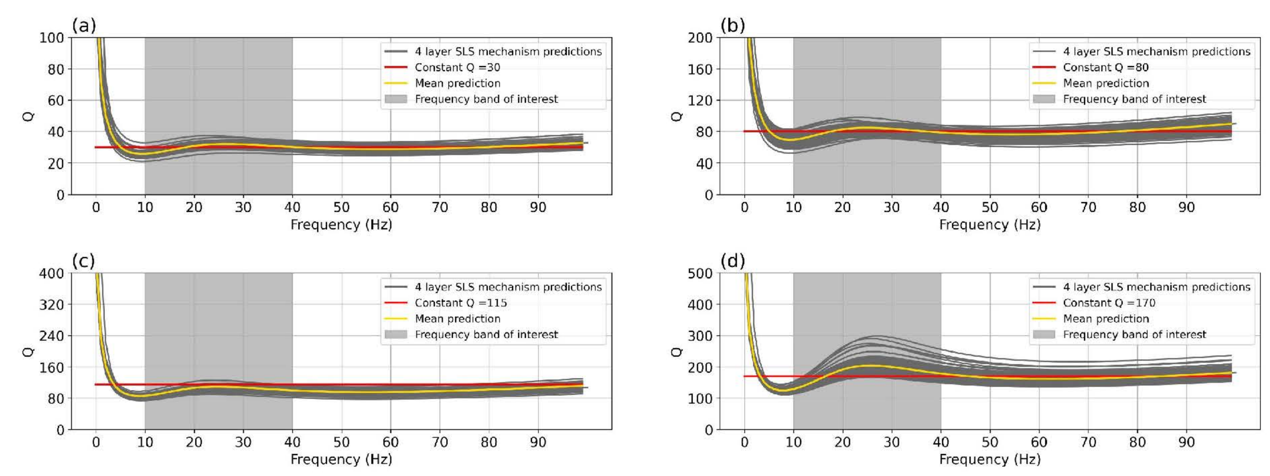

Fig4. The Q spectrums and the uncertainty quantification predicted by the neural network using 3 layers of the GSLS mechanism.

Fig5. Phase velocity variation with respect to a frequency band of 1Hz - 100Hz with Q values of 60, 80, 100. (a) Reference frequency 10Hz. (b) Reference frequency 20 Hz.

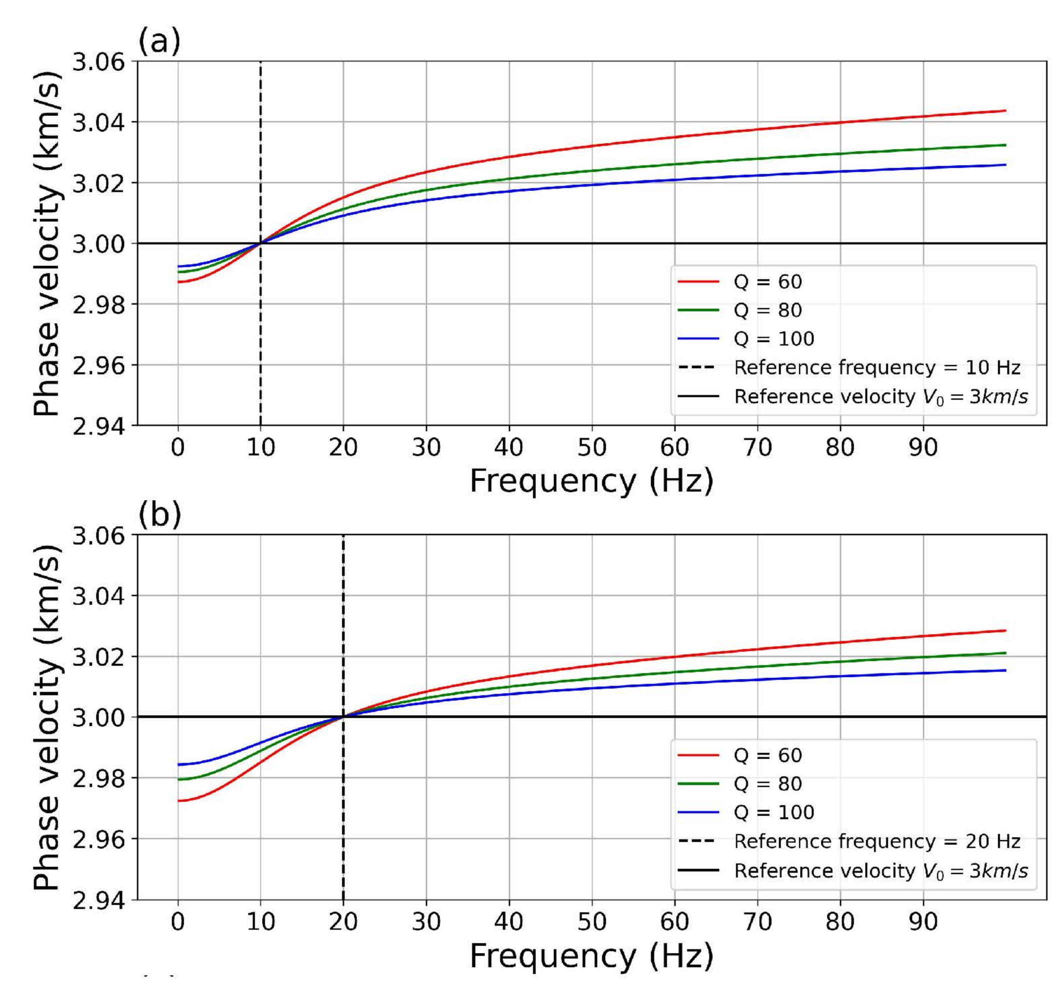

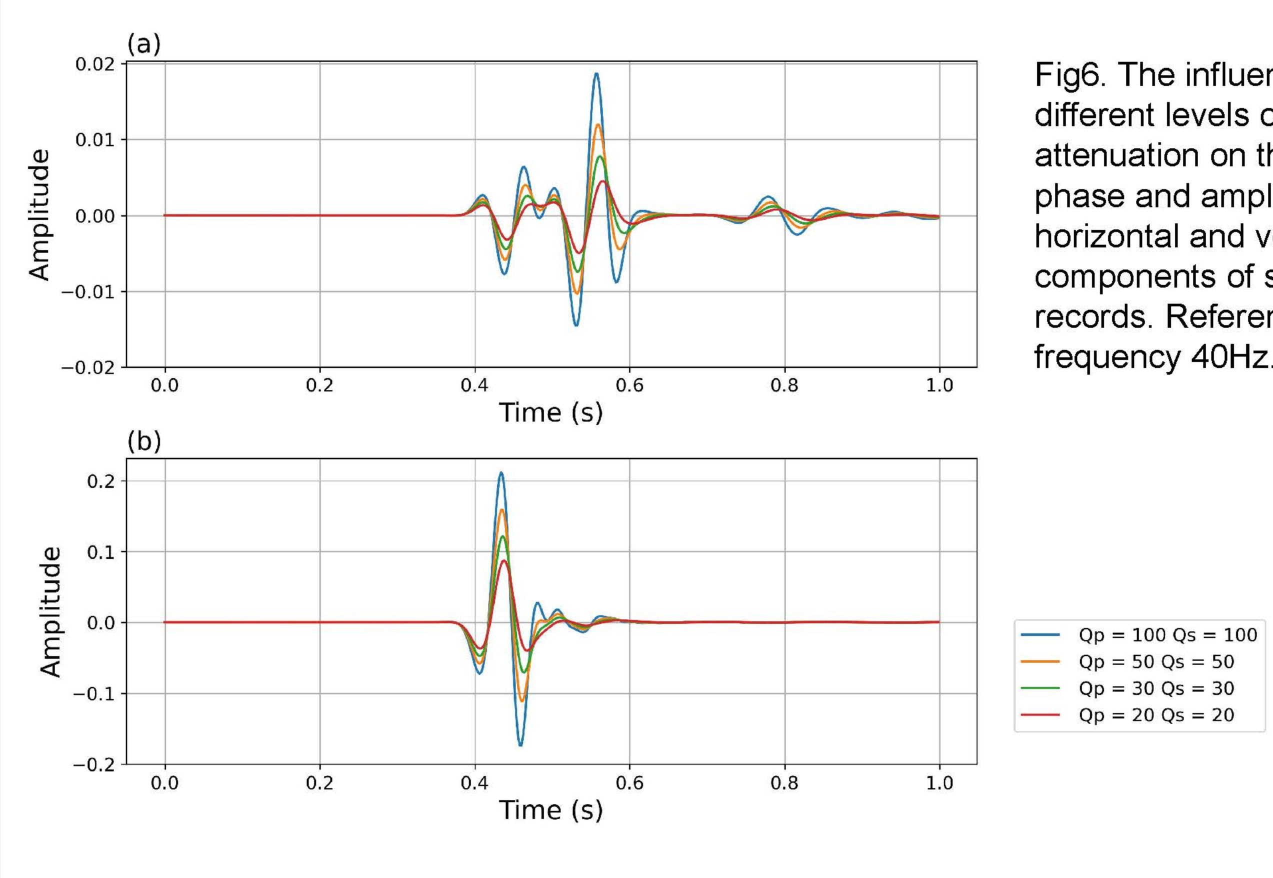

Fig6. The influence of different levels of attenuation on the phase and amplitude of horizontal and vertical components of seismic records. Reference frequency 40Hz.

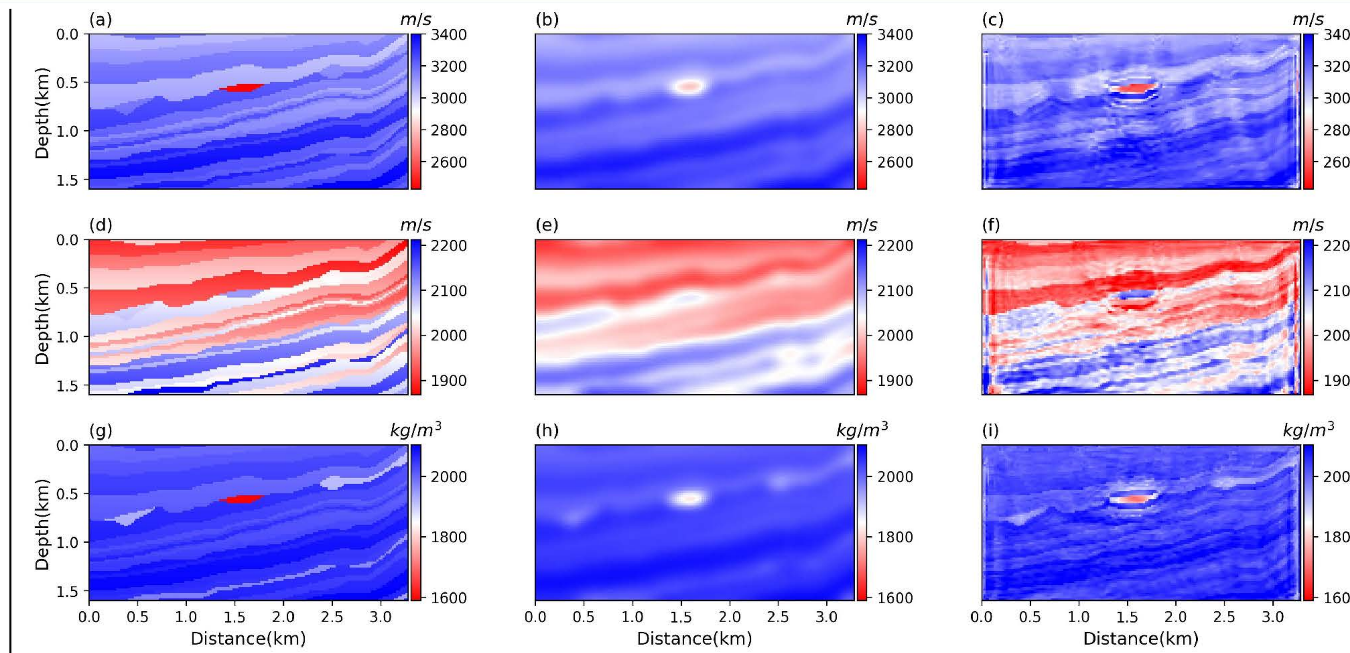

Fig7. Part of the Marmousi model Vp, Vs, and ρ viscoelastic FWI. (a), (d) and (g) are the true models for Vp, Vs, and ρ. (b), (e) and (h) are the initial models. (c), (f) and (i) are the inversion results for Vp, Vs, and ρ, respectively.

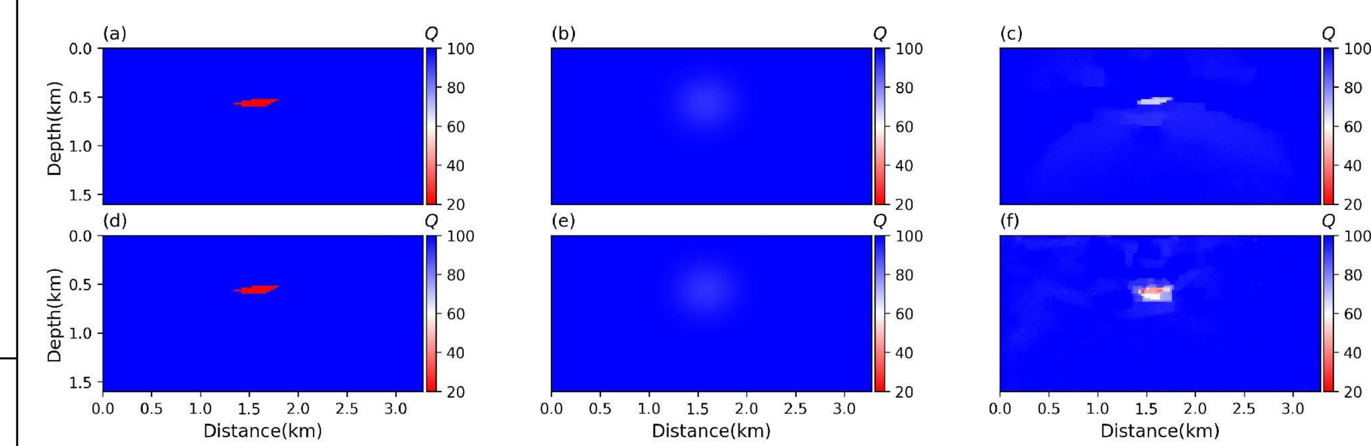

Fig8. Part of the Marmousi model Qp, Qs viscoelastic FWI. (a) and (d) are the true models for Qp and Qs, respectively. (b), (e) are the initial models for Qp and Qs, respectively. (c) and (f) are the inversion results for Qp and Qs, respectively.

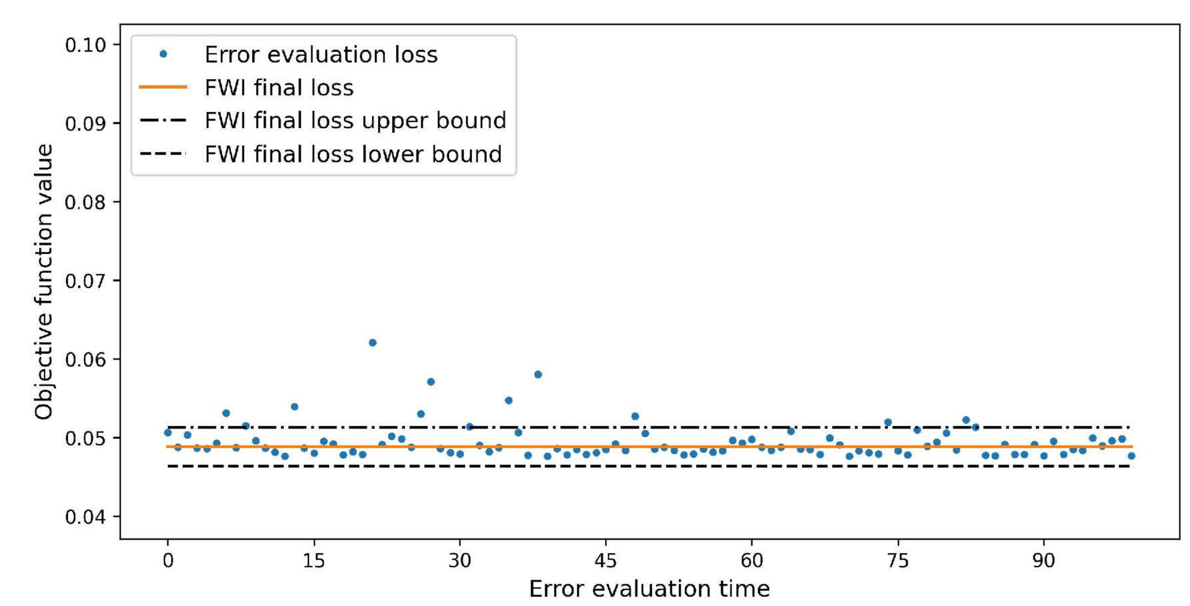

Fig9. The loss values of 100 times modeling error evaluation are plotted as blue points. The yellow line represents the FWI objective function value at the last iteration. If the elastic models evaluated with the modeling error detection calculation fall between the upper and lower bound of the FWI final loss, these elastic models will be considered.

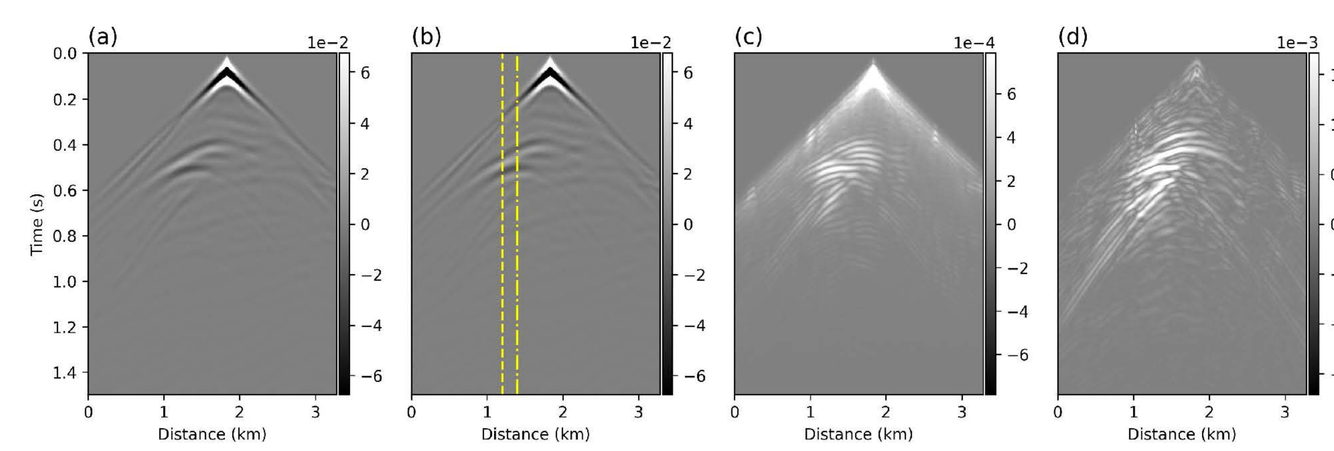

Fi10. Modeling error evaluation of the Marmousi model. (a) The observed record at 1000 m of the model. (b) Synthetic data from the final iteration of FWI. (c) The standard deviation record of the collected Dtest, is regarded as the modeling error. (d) Absolute error between (a) and (b).

NSERC CRSNG
UNIVERSITY OF CALGARY
FACULTY OF SCIENCE
Department of Geoscience
, and Environment
Carbon Management Canada